

The thawing dark energy dynamics: Can we detect it?

S. Sen,¹ A. A. Sen,¹ and M. Sami¹

¹*Centre for Theoretical Physics, Jamia Millia Islamia, New Delhi-110025, India*

We consider different classes of scalar field models including quintessence, and tachyon scalar fields with a variety of generic potential belonging to thawing type. We focus on observational quantities like Hubble parameter, luminosity distance as well as quantities related to the Baryon Acoustic Oscillation measurement. Our study shows that with present state of observations, one can not distinguish amongst various models which in turn can not be distinguished from cosmological constant. This leads to a conclusion that there is a thin chance to observe the dark energy metamorphosis in near future.

PACS numbers: 98.80 Cq

I. INTRODUCTION

The fact that our universe is currently going through an accelerated phase of expansion is one of the most significant discoveries [1] in physics in recent times that can have far reaching implications for fundamental theories of physics. Late time cosmic acceleration can be fueled either by assuming the presence of an exotic fluid with large negative pressure known as *dark energy* or by modifying gravity itself. The simplest candidate of dark energy is provided by cosmological constant with equation of state parameter $w = -1$. However, the model based upon cosmological constant is plagued with the fine tuning and cosmic coincidence problems (See Ref [2] for a nice review).

Scalar field models with generic features can alleviate the fine tuning and coincidence problems and provide an interesting alternative to cosmological constant [3]. The simplest generalization of cosmological constant is provided by a scalar field with linear potential [4]. Its evolution begins from the locking regime (due to large Hubble damping) where it mimics the cosmological constant like behavior. At late times, the field starts rolling and since the potential has no minimum, the model leads to a collapsing universe with a finite history.

The more complicated scalar field models can broadly be classified into two categories- fast roll and slow roll models dubbed freezing and thawing models [5]. In case of the fast roll models, the potential is steep allowing the scalar field to mimic the background being subdominant for most of the evolution history. Only at late times, the field becomes dominant and drives the acceleration of the universe. Such solutions are referred to as *trackers*.

Slow-roll models are those for which the field kinetic energy is much smaller than its potential energy. It usually has a sufficiently flat potential similar to an inflaton. At early times, the field is nearly frozen at $w = -1$ due to the large Hubble damping. Its energy density is nearly constant and its contribution to the total energy density of the universe is also nearly negligible. But as radiation/matter rapidly dilutes due to the expansion of the universe and the background energy density becomes comparable to field energy density, the field breaks away

from its frozen state evolving slowly to the region with larger values of equation of state parameter. In this case, however, one needs to have some degree of fine tuning of the initial conditions in order to achieve a viable late time evolution.

Recent observations suggest that the equation of state parameter for dark energy does not significantly deviate from $w = -1$ around the present epoch [6]. This type of equation of state can be easily obtained in dynamical models represented by thawing scalar fields. This fact was exploited in Ref [7] which examined quintessence models with nearly flat potentials satisfying the slow-roll conditions. It was shown that under the slow-roll conditions, a scalar field with a variety of potentials $V(\phi)$ evolve in a similar fashion and one can derive a generic expression for equation of state for all such scalar fields. This result was later extended to the case of phantom [8] and tachyon scalar fields [9]. It was demonstrated that under slow-roll conditions, all of them have identical equation of state and hence can not be distinguished, at least, at the level of background cosmology. The crucial assumption, for arriving at this important conclusion was the fulfillment of the slow-roll condition for the field potentials.

In this paper, we relax the assumption of slow roll but assume that the scalar field is of thawing type i.e it is initially frozen at $w = -1$ due to large Hubble damping. With non-negligible matter contribution, this does not necessarily mean the small value for $V_{,\phi}/V$ which is the usual slow-roll parameter for inflaton. We, rather, assume that the slow-roll condition is highly broken such that $V_{,\phi}/V \sim 1$. In this case, we need to fine tune the initial conditions to match the observational value of the present day dark energy density which is a characteristic feature of any thawing model. With this choices, we study the evolution of a variety of scalar field models having both canonical and non-canonical kinetic terms. We particularly focus on the observational quantities like Hubble parameter, luminosity distance as well as quantities related to the Baryon Acoustic Oscillation (BAO) measurement.

II. THAWING SCALAR FIELD

In what follows, we shall assume that the dark energy is described by a minimally-coupled scalar field, ϕ , with equation of motion

$$\ddot{\phi} + 3H\dot{\phi} + V_{,\phi} = 0 \quad (1)$$

where the Hubble parameter H is given by

$$H = \left(\frac{\dot{a}}{a} \right) = \sqrt{\rho/3}. \quad (2)$$

Here ρ is the total energy density in the universe. We model a flat universe containing only matter and a scalar field, so that $\Omega_\phi + \Omega_M = 1$.

Equation (1) indicates that the field rolls downhill in the potential $V(\phi)$, but its motion is damped by a term proportional to H . The equation of state parameter w is given by $w = p_\phi/\rho_\phi$ where the pressure and density of the scalar field have the form

$$p = \frac{\dot{\phi}^2}{2} - V(\phi), \quad (3)$$

$$\rho = \frac{\dot{\phi}^2}{2} + V(\phi) \quad (4)$$

Observations suggest a value of w near -1 around the present epoch. We adopt a similar technique as followed in references [7, 8] and define the variables x , y , and λ as

$$x = \phi'/\sqrt{6}, \quad (5)$$

$$y = \sqrt{V(\phi)/3H^2}, \quad (6)$$

$$\lambda = -\frac{1}{V} \frac{dV}{d\phi}, \quad (7)$$

where prime as usual denote the derivative with respect to $\ln a$: e.g., $\phi' \equiv a(d\phi/da)$

Then contribution of the kinetic energy and potential energy of the scalar field to the fractional density parameter Ω_ϕ are represented by x^2 and y^2 such that,

$$\Omega_\phi = x^2 + y^2, \quad (8)$$

while the equation of state is given by,

$$\gamma \equiv 1 + w = \frac{2x^2}{x^2 + y^2}. \quad (9)$$

In terms of the variables x , y , and λ , evolution equations (1) and (2) take the autonomous form

$$x' = -3x + \lambda\sqrt{\frac{3}{2}}y^2 + \frac{3}{2}x[1 + x^2 - y^2], \quad (10)$$

$$y' = -\lambda\sqrt{\frac{3}{2}}xy + \frac{3}{2}y[1 + x^2 - y^2], \quad (11)$$

$$\lambda' = -\sqrt{6}\lambda^2(\Gamma - 1)x, \quad (12)$$

where

$$\Gamma \equiv V \frac{d^2V}{d\phi^2} / \left(\frac{dV}{d\phi} \right)^2. \quad (13)$$

We now rewrite these equations, changing the dependent variables from x and y to the observable quantities Ω_ϕ and γ given by equations (8) and (9). To make this transformation, we assume that $x' > 0$; our results generalize trivially to the opposite case. In terms of Ω_ϕ and γ the above set of equation become

$$\gamma' = -3\gamma(2 - \gamma) + \lambda(2 - \gamma)\sqrt{3\gamma\Omega_\phi}, \quad (14)$$

$$\Omega'_\phi = 3(1 - \gamma)\Omega_\phi(1 - \Omega_\phi), \quad (15)$$

$$\lambda' = -\sqrt{3}\lambda^2(\Gamma - 1)\sqrt{\gamma\Omega_\phi}. \quad (16)$$

This is an autonomous system of equations involving the observable parameter γ and Ω_ϕ . Given the initial conditions for γ , Ω_ϕ and λ , one can solve this system of equation numerically for different potentials. As we mention earlier, we are interested in thawing models i.e models for which the equation of state is initially frozen at $w = -1$. Hence $\gamma = 0$ initially for our purpose. We also do not assume slow-roll conditions for the scalar field potentials rather we consider situations for which it is broken strongly i.e $\lambda_{initial} \sim 1$. We should mention that for models where slow-roll condition is satisfied i.e. $\lambda \ll 1$, it has been already shown that all such models have an identical equation of state as a function of scale factor [7, 8]. In general the contribution of the scalar field to the total energy density of the universe is insignificant at early times, nevertheless one has to fine tune the initial value of Ω_ϕ in order to have its correct contribution at present. This is the fine tuning one needs to have in a thawing models. With these initial conditions we evolve the above system of equations from redshift $z = 1000$ (or $a = 10^{-3}$) till the present day $z = 0$ ($a = 1$). We consider various types of potentials e.g $V = \phi$, $V = \phi^2$, $V = e^\phi$ and $V = \phi^{-2}$, characterized by $\Gamma = 0, \frac{1}{2}, 1$ and $\frac{3}{2}$ respectively. We have taken two sets of solution such that $\Omega_\phi = 0.7$ and $\Omega_\phi = 0.75$ at the present epoch for all chosen values of Γ .

We also consider the Pseudo-Nambu Goldstone Boson (PNGB) model [10]. (For a recent discussion, see Ref. [11] and references therein). This model is characterized by the potential

$$V(\phi) = M^4[\cos(\phi/f) + 1], \quad (17)$$

Alam et al.,[12] have previously considered such type of potential to see whether dark energy is decaying or not.

We have chosen f to be 1 for our purpose without any loss generality.

As mentioned before, tachyon field is of interest in cosmology. There have been several investigations using this field as a dark energy candidate [14]. In what follows, we shall repeat the above presented analysis for tachyon field.

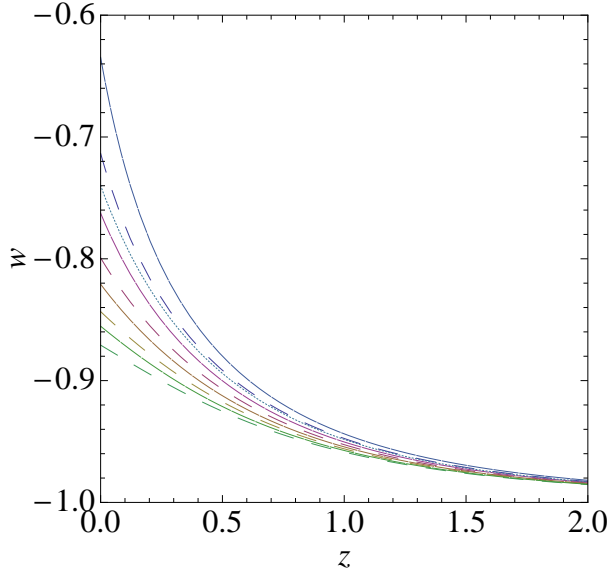


FIG. 1: Plot of equation of state w vs. redshift for different scalar field and tachyon models. Solid curves represent different Tachyonic models with $V(\phi) = \phi, \phi^2, e^\phi, \phi^{-2}$ respectively from top to bottom, Dashed curves from top to bottom represent different scalar field models with same potentials as in tachyon. Dotted curve represents PNGB model. $\Omega_m = 0.3$.

III. THAWING TACHYON FIELD

The tachyon field is specified by the Dirac-Born-Infeld (DBI) type of action [13]

$$\mathcal{S} = \int -V(\phi) \sqrt{1 - \partial^\mu \phi \partial_\mu \phi} \sqrt{-g} d^4x. \quad (18)$$

In FRW background, the pressure and energy density of the tachyon field ϕ are given by

$$p_\phi = -V(\phi) \sqrt{1 - \dot{\phi}^2} \quad (19)$$

$$\rho_\phi = \frac{V(\phi)}{\sqrt{1 - \dot{\phi}^2}} \quad (20)$$

The equation of motion which follows from (18) is

$$\ddot{\phi} + 3H\dot{\phi}(1 - \dot{\phi}^2) + \frac{V'}{V}(1 - \dot{\phi}^2) = 0 \quad (21)$$

where H is the Hubble parameter. The evolution equations can be cast in the following autonomous form for the convenient use

$$x'_t = -(1 - x_t^2)(3x_t - \sqrt{3}\lambda_t y_t) \quad (22)$$

$$y'_t = \frac{y_t}{2} \left[-\sqrt{3}\lambda_t x_t y_t - \frac{3(1 - x_t^2)y_t^2}{\sqrt{1 - x_t^2}} + 3 \right] \quad (23)$$

$$\lambda'_t = -\sqrt{3}\lambda_t^2 x_t y_t \left(\Gamma - \frac{3}{2} \right) \quad (24)$$

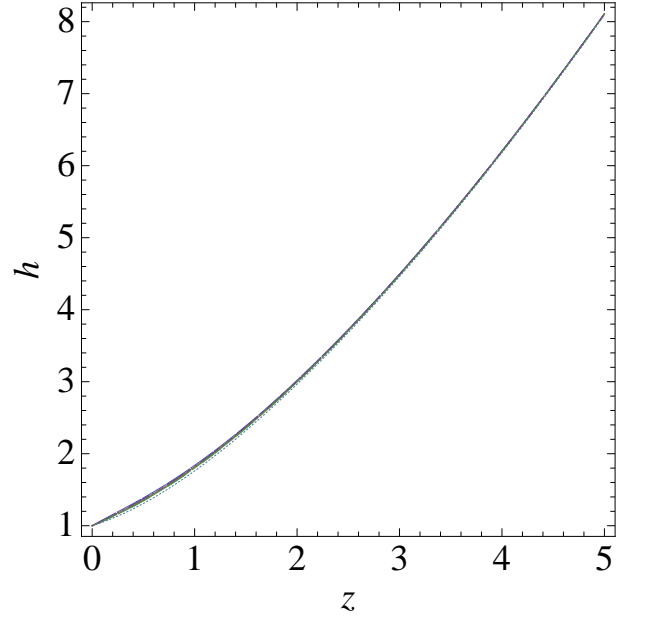


FIG. 2: Plot of $h(a) = \frac{H(a)}{H_0}$ vs. redshift for different models as well as for Λ CDM. $\Omega_{m0} = 0.3$. As one can see, all of them have similar behaviour.

with x_t, y_t, λ_t and Γ defined as

$$x_t = \dot{\phi}, \quad y_t = \frac{\sqrt{V(\phi)}}{\sqrt{3}H}, \quad \lambda_t = -\frac{V_\phi}{V^{\frac{3}{2}}}, \quad \Gamma = V \frac{V_{\phi\phi}}{V_\phi^2} \quad (25)$$

where prime again denotes the derivative with respect to $\ln(a)$. We would further use the following definitions for the tachyon field as we did in case of thawing quintessence

$$\Omega_\phi = \frac{y^2}{\sqrt{1 - x^2}}, \quad \gamma \equiv 1 + w = \dot{\phi}^2, \quad (26)$$

where $w = \frac{p_\phi}{\rho_\phi}$ is the equation of state for the tachyon field. One can now express the autonomous equations through them:

$$\gamma' = -6\gamma(1 - \gamma) + 2\sqrt{3}\gamma\Omega_\phi\lambda_t(1 - \gamma)^{\frac{5}{4}} \quad (27)$$

$$\Omega'_\phi = 3\Omega_\phi(1 - \gamma)(1 - \Omega_\phi) \quad (28)$$

$$\lambda'_t = -\sqrt{3}\gamma\Omega_\phi\lambda_t^2(1 - \gamma)^{\frac{1}{4}}\left(\Gamma - \frac{3}{2}\right) \quad (29)$$

We adopt a similar treatment to solve the above set of equation (27)-(29) as we had done in the earlier case. Infact, we even consider similar kind of potentials for tachyon fields as well, i.e. $V = \phi, V = \phi^2, V = e^\phi$ and $V = \phi^{-2}$, characterized by $\Gamma = 0, \frac{1}{2}, 1$ and $\frac{3}{2}$ respectively along with the initial conditions for $\lambda_{tinitial}$ to be 1 and $\gamma_{initial} \sim 0$. Here also we take two solutions set for all Γ 's, with two different initial conditions of Ω_ϕ such that at present it contributes 70% and 75% of the total energy share. Before discussing our result, we want to point that the system of equations (14)-(16) and (27)-(29) for scalar field and tachyon field respectively are completely

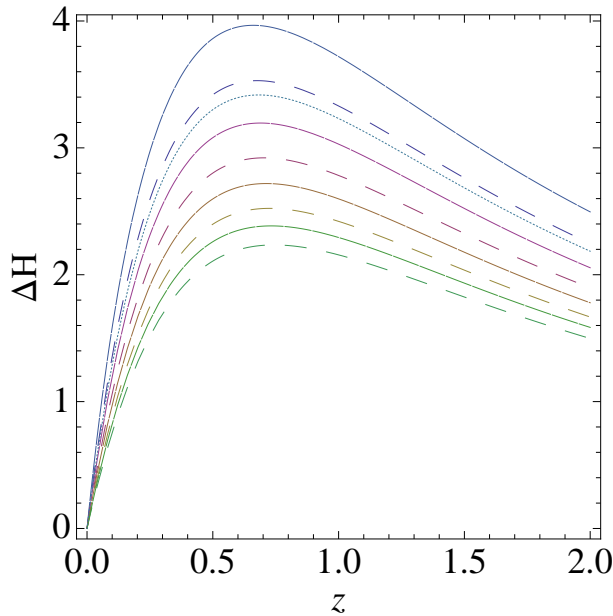


FIG. 3: Plot of ΔH (explained in the text) vs. redshift for different models. Solid curves represent different Tachyonic models with $V(\phi) = \phi, \phi^2, e^\phi, \phi^{-2}$ respectively from top to bottom, Dashed curves from top to bottom represent different scalar field models with same potentials as in tachyon. Dotted curve represents PNGB model. $\Omega_{m0} = 0.3$.

different. Hence *a priori* one expects to have different evolutions for different potentials as well as for scalar and tachyon fields.

Once we know the solution for $\Omega_\phi(a)$ by solving either (14)-(16) or (27)-(29), we can easily find the behavior of the Hubble parameter which, in terms of Ω_ϕ , can be expressed as

$$h^2(a) = \frac{H^2(a)}{H_0^2} = \frac{1 - \Omega_{\phi 0}}{1 - \Omega_\phi} a^{-3}, \quad (30)$$

where H_0 and $\Omega_{\phi 0}$ are the present day values for the Hubble parameter and the dark energy density parameter. This is the most important parameter as all the observable quantities involving background cosmology can be constructed from this. Moreover there are independent observational constraint on this parameter itself. We should mention that in this approach, one does not need to know the equation of state ($\gamma(a) = 1 + w(a)$) to construct the observational quantities although its effect comes through the solutions of Eqs.(14)-(16) or (27)-(29).

IV. RESULTS

Let us now discuss the results of our investigations. We first plot the behaviours of the equation of state $w(a)$ for different models in fig1. It shows that the equation of states of different fields with different potentials behave

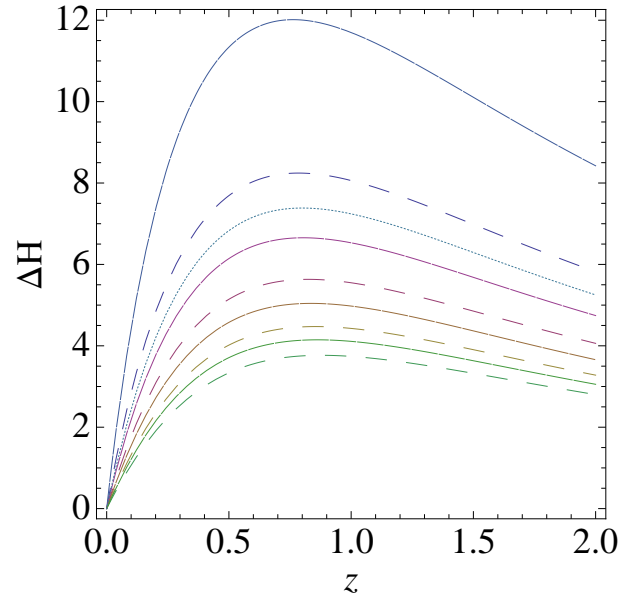


FIG. 4: Plot of ΔH (explained in the text) vs. redshift for different models. Solid curves represent different Tachyonic models with $V(\phi) = \phi, \phi^2, e^\phi, \phi^{-2}$ respectively from top to bottom, Dashed curves from top to bottom represent different scalar field models with same potentials as in tachyon. Dotted curve represents PNGB model. $\Omega_{m0} = 0.25$.

differently as one approaches the present day although in the past their behaviours are almost identical. We should emphasize that we have assumed the violation of slow-roll condition, i.e $\lambda_{initial} \sim 1$. Hence this is expected. With slow-roll condition satisfied i.e $\lambda_i \ll 1$, it has already been shown that that models with different potentials have the identical $w(a)$ both for scalar and tachyon field [7, 8, 9].

Next we show the behaviour of the Hubble parameter for different cases. With different behaviours for $w(a)$ as shown in fig1, one would expect to have different behaviours for Hubble parameter also. But they are completely indistinguishable as shown in fig 2. In this figure, we have also plotted $h(a)$ for Λ CDM. As one can see, we can not distinguish between individual models as well as different models with Λ CDM. It is interesting to see that despite having completely different behaviour for equation of state, all the models have identical evolution for the Hubble parameter. This is crucial as all the observational quantities are constructed out of $h(a)$ at least for background cosmology. In recent past, estimates of $H(z)$ were derived by Simon, Verde and Jimenez using passively evolving galaxies [15] (also see Ref[16]). Keeping this in mind, we next plot the different $\Delta H = H_{field} - H_{\Lambda CDM}$ for each of our model in fig 3 and fig 4 for two different values of Ω_{m0} (0.7 and 0.75) respectively. For this, we use the prior $H_0 = 73 \pm 3 \text{ km s}^{-1} \text{ Mpc}^{-1}$. If one now compares the ΔH with the error bars for the $H(Z)$ measurements as quoted in Ref[15, 16], one sees that with $\Omega_{m0} = 0.3$, one can not

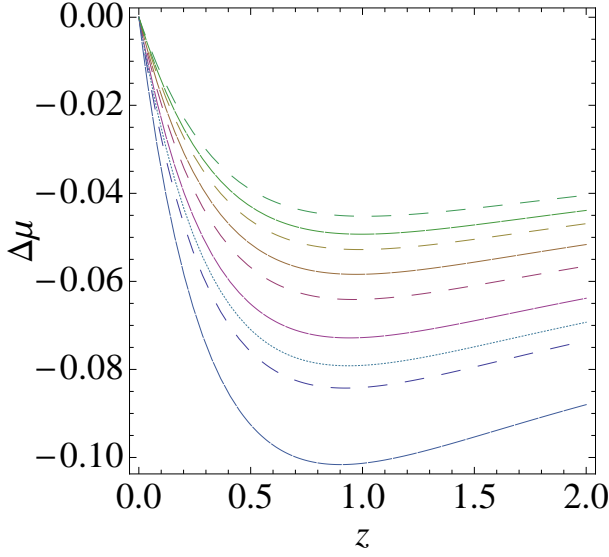


FIG. 5: Plot of $\Delta\mu$ (explained in the text) vs. redshift for different models. Solid curves represent different Tachyonic models with $V(\phi) = \phi, \phi^2, e^\phi, \phi^{-2}$ respectively from top to bottom, Dashed curves from top to bottom represent different scalar field models with same potentials as in tachyon. Dotted curve represents PNGB model. $\Omega_{m0} = 0.3$.

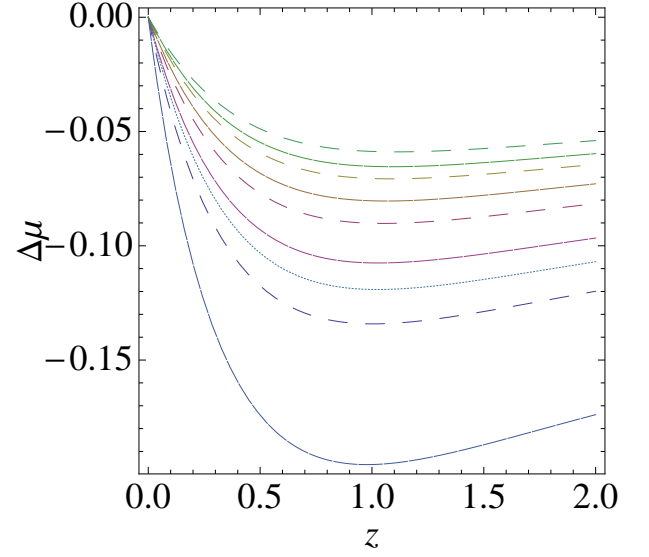


FIG. 6: Plot of $\Delta\mu$ (explained in the text) vs. redshift for different models. Solid curves represent different Tachyonic models with $V(\phi) = \phi, \phi^2, e^\phi, \phi^{-2}$ respectively from top to bottom, Dashed curves from top to bottom represent different scalar field models with same potentials as in tachyon. Dotted curve represents PNGB model. $\Omega_{m0} = 0.25$.

distinguish all these models with Λ CDM. With smaller values of Ω_{m0} , e.g $\Omega_{m0} = 0.25$, the difference gets larger, and the models that can be distinguished are those with linear potentials for both ordinary scalar fields as well as for tachyon. For other models including PNGB, still the error bars are not so tight to distinguish them from Λ CDM. The other interesting thing which one notices from both these figures, is that the difference is maximum in the redshift range 0.5 to 1. Hence having more data points for higher redshifts is not useful as long as one wants to distinguish different models from Λ CDM. Rather low redshift measurements is more vital more this purpose.

Next we consider the Supernova Type-Ia observation which is one of the direct probes for late time acceleration. It measures the apparent brightness of the supernovae as observed by us which is related to the luminosity distance $d_L(z)$ defined as

$$d_L = (1+z) \int_0^z \frac{dz'}{H(z')}. \quad (31)$$

Model	$V(\phi)$	$D_{V\phi} - D_{V\Lambda}$ for $\Omega_\phi = 0.70$
Thawing Model	ϕ	-0.01464
Thawing model	ϕ^2	-0.01156
Thawing model	e^ϕ	-0.00972
Thawing model	$\frac{1}{\phi^2}$	-0.00843
Scalar field	$M^4[\cos \phi + 1]$ (PNGB)	-0.01398
Tachyon	ϕ	-0.01715
Tachyon	ϕ^2	-0.01291
Tachyon	e^ϕ	-0.01062
Tachyon	$\frac{1}{\phi^2}$	-0.00911

Table 1

With this, one constructs the distance modulus μ which is experimentally measured:

$$\mu = m - M = 5 \log \frac{d_L}{Mpc} + 25, \quad (32)$$

where m and M are the apparent and absolute magnitudes of the supernovae which are logarithmic measure of flux and luminosity respectively. In fig 5 and Fig6, we plot the difference $\Delta\mu = \mu_\phi - \mu_{\Lambda CDM}$ for each model. As one can see the difference with Λ CDM is highest with linear potential for both ordinary scalar field and tachyon. As one decreases the value of Ω_{m0} , the difference increases. Moreover, similar to the behaviour of ΔH , the difference is most prominent in the redshift range between 0.5 to 1. Let us compare our result with the latest Union compilation of the supernova data [17]. If one

compare $\Delta\mu$ with the error bars in this data set, one can see that the only models those are distinguishable with Λ CDM are the models with linear potentials and that too for lower Ω_{m0} value.

Model	$V(\phi)$	$D_{V\phi} - D_{V\Lambda}$ for $\Omega_\phi = 0.75$
ThawingModel	ϕ	-0.02369
Thawing model	ϕ^2	-0.01667
Thawing model	e^ϕ	-0.01332
Thawing model	$\frac{1}{\phi^2}$	-0.01121
Scalar field	$M^4[\cos\phi + 1]$ (PNGB)	-0.02156
Tachyon	ϕ	-0.03313
Tachyon	ϕ^2	-0.01951
Tachyon	e^ϕ	-0.01498
Tachyon	$\frac{1}{\phi^2}$	-0.01235

Table 2

Another observational probe that has been widely used in recent times to constraint dark energy models is related to the data from the Baryon Acoustic Oscillations measurements[18]. In this case, one needs to calculate the parameter D_V which is related to the angular diameter distance as follows

$$D_V(z_{BAO}) = \left[\frac{z_{BAO}}{H(z_{BAO})} \left(\int_0^{z_{BAO}} \frac{dz}{H(z)} \right)^2 \right]^{1/3} \quad (33)$$

For BAO measurements we calculate the ratio $D_V(z = 0.35)/D_V(z = 0.20)$. As shown in [19] this ratio is a relatively model independent quantity and has a value 1.812 ± 0.060 . For our case, we calculate the difference of this ratio between any scalar field model and Λ CDM model. In tables 1 & 2, we quote our result for two different values for $\Omega_{m0} : \Omega_m = 0.3, \Omega_{m0} = 0.25$.

As one can see from the results quoted in these two tables, with current BAO measurements, it is hard to distinguish all these models with Λ CDM. One has to decrease the error bars at least by fifty percent for this purpose.

V. CONCLUSION

In this paper, we have studied the general class of thawing models with both quintessence and tachyon type scalar fields without assuming slow-roll conditions for the potentials of these fields. Our investigations show that the overall Hubble parameter has almost identical behavior for all these models and also matches with its counterpart corresponding to Λ CDM inspite of the fact that the equation of states for different models behave quite differently. Since all the observable quantities related to background evolution, are constructed out of $H(z)$, it is practically impossible to distinguish these models from Λ CDM using the current data. While analyzing the observational constraints, we used supernova and BAO data along with the information on Hubble parameter measurements. Our analysis shows that with smaller values of Ω_{m0} , it is easier to distinguish amongst the various models. An interesting outcome of our study is related to the redshift range showing distinguished features. We find that the behavior of thawing dynamics around $z = 0.5$ to $z = 1$ is most sensitive to deviation from Λ CDM. Hence the future observations should concentrate more on this particular range so as to decrease the error bars significantly.

VI. ACKNOWLEDGEMENT

A.A.S acknowledges the financial support provided by the University Grants Commission, Govt. Of India, through major research project grant (Grant No:33-28/2007(SR)). S.S acknowledges the financial support provided by University Grants Commission, Govt. Of India through the D.S.Kothari Post Doctoral Fellowship.

-
- [1] R. A. Knop et al., Ap.J. **598**, 102 (2003); A. G. Riess, et al., Ap.J. **607**, 665 (2004).
[2] E. J. Copeland, M. Sami and S. Tsujikawa, Int.J.Mod.Phys.D **15**, 1753 (2006); M. Sami, arXiv:0904.3445; V. Sahni and A. A. Starobinsky, Int.J.Mod.Phys.D **9**, 373 (2000); T. Padmanabhan, Phys.Rep. **380**, 235 (2003); E. V. Linder, astro-ph/0704.2064; J. Frieman, M. Turner and D. Huterer, arXiv:0803.0982; R. Caldwell and M. Kamionkowski, arXiv:0903.0866; A. Silvestri and M. Trodden, arXiv:0904.0024.
[3] B. Ratra and P. J. E. Peebles, Phys.Rev.D **37**, 3406 (1988); R. R. Caldwell, R. Dave and P. J. Steinhardt, Phys.Rev.Lett. **80**, 1582 (1998); A. R. Liddle and R. J. Scherrer, Phys.Rev.D **59**, 023509 (1999); P. J. Steinhardt, L. Wang and I. Zlatev, Phys.Rev.D **59**, 123504 (1999);
[4] R. Kallosh, et al., JCAP **0310**, 015 (2003); P. P. Avelino, et al., Phys.Rev.D **70**, 083506 (2004).
[5] R. R. Caldwell and E. V. Linder, Phys.Rev.Lett. **95**, 141301 (2007).
[6] W. M. Vassey, et al., Ap.J. **666**, 694 (2007); T. M. Davis, et al., Ap.J **666**, 716 (2007).
[7] R. J. Scherrer and A. A. Sen, Phys.Rev.D **77**, 083515 (2008).
[8] R. J. Scherrer and A. A. Sen, Phys.Rev.D **78**, 067303 (2008).
[9] A. Ali, M. Sami and A. A. Sen, arXiv:0904.1070 [astro-

- ph.CO].
- [10] J. A. Frieman, et al., Phys.Rev.Lett. **75**, 2077 (1995).
 - [11] A. Abrahamse, et al., arXiv:0712.2879.
 - [12] U. Alam, V. Sahni and A.A. Starobinsky, JCAP **0304**, 002 (2003).
 - [13] A. Sen, JHEP **9910**, 008 (2002); A. Sen, Mod.Phys.Lett.A **17**, 1797 (2002); M. R. Garousi, Nucl. Phys. B**584**, 284 (2000); E. A. Bergshoeff, M. de Roo, T. C. de Wit, E. Eyras, S. Panda, JHEP **0005**, 009 (2000); J. Kluson, Phys.Rev. D **62**, 126003 (2000); D. Kutasov and V. Niarchos, Nucl.Phys. B **666**, 56 (2003).
 - [14] E. J. Copeland, M. R. Garousi, M. Sami, S. Tsujikawa, Phys. Rev. **D71**, 043003 (2005); S. Tsujikawa and M. Sami, Phys. Lett. **B603**,113(2004); M. Sami, N. Savchenko and A. Toporensky, Phys. Rev. **D70**, 123528(2004); G. N. Felder, Lev Kofman and A. Starobinsky, JHEP **0209**,026(2002); J. S. Bagla, H. K. Jassal and T. Padmanabhan, Phys. Rev. D **67**, 063504 (2003); L. R. W. Abramo and F. Finelli, Phys. Lett. B **575**, 165 (2003); J. M. Aguirregabiria and R. Lazkoz, Phys. Rev. D **69**, 123502 (2004);
 - [15] J. Simon, L. Verde, R. Jimenez, Phys.Rev.D **71**, 123001 (2005).
 - [16] L. Samushia and B. Ratra, Ap.J. **650**, L5 (2006).
 - [17] M. Kowalski, et al., Ap.J. **686**, 749 (2008).
 - [18] D. J. Eisensetin, et al., Ap.J. **633**, 560 (2005).
 - [19] W. J. Percival, et al., MNRAS **381**, 1053 (2007).